

The use of softer X-rays in the structure elucidation of microporous materials

M. Helliwell,^{a*} R. H. Jones,^b V. Kaucic^c and N. Z. Logar^c

^aSchool of Chemistry, The University of Manchester, Manchester M13 9PL, UK, ^bSchool of Molecular Sciences, University of Keele, Keele, Staffordshire ST5 5BG, UK, and ^cThe National Institute of Chemistry, Hajdrihova 19, 1000 Ljubljana, Slovakia.
E-mail: madeleine.helliwell@man.ac.uk

Microporous materials, such as zeolites and aluminophosphates, have many applications as molecular sieves and shape-selective catalysts. This is due to their three-dimensional frameworks, which contain regular pores and channels, to their high acidity, arising from Brønsted and Lewis acid active sites, and to the incorporation of transition metal atoms into framework sites. This review firstly provides an introduction into the nature and properties of these materials, and their important applications; the difficulties in their full characterization and possible methods of elucidating their structures are then outlined; finally, methods of characterization, utilizing 'softer X-rays' are introduced. The first method is the determination of low concentrations of transition metals, incorporated into the frameworks using single crystal anomalous dispersion crystallography; synchrotron radiation is used to tune to the absorption edge of the metal atom in question, in order to change its signal relative to that of the rest of the structure, thereby allowing the pinpointing of its positions and the determination of its concentration at each site in the framework. Secondly, the use of longer wavelengths in powder diffraction studies is described, which, by stretching out the powder pattern, thereby reduces the overlapping of the diffraction peaks, thus allowing the structure to be solved by conventional direct methods. Finally, the use of X-ray absorption spectroscopy to determine the metal incorporation and the nature of coordination at the metal atom sites, in Mn silicalite-1 and FAPO-36, are described.

1. Introduction

Microporous materials are crystalline solids that contain interconnected cavities or channels with pores of molecular dimensions typically from 3 to 20 Å. The large internal surface area and void volumes with extremely narrow pore size distribution and functional centres dispersed over the surface make microporous solids highly active materials. Over the last decade, there has been a dramatic increase in the synthesis, characterization and application of novel microporous materials (Cheetham *et al.*, 1999). They are mostly used as catalysts and catalyst supports in the petroleum industry for various types of shape-selective conversion and separation reactions (Marcilly, 2001; Kaucky *et al.*, 2000). They form the basis of new environmentally friendly technologies involving waste treatment, energy storage and novel reactions that arise from their unique structural and surface physicochemical properties, such as excellent adsorption and ion-exchange capacities. Among the very recent applications of microporous materials

are optical-electronic devices, biological materials and implants, sensors and membranes for gas separation and gas storage (reviewed by Marlow *et al.*, 2002).

Microporous materials range from inorganic zeolites to zeolite-like aluminophosphates and gallophosphates or the recently discovered inorganic/organic hybrids (Ferey, 2001; Rajic *et al.*, 2003). Zeolites, which represent the largest group of microporous materials, are crystalline inorganic polymers based on a three-dimensional arrangement of SiO₄ and AlO₄ tetrahedra connected through their O atoms to form large negatively charged lattices with Brønsted and Lewis acid sites. These negative charges are balanced by extra-framework alkali and/or alkaline earth cations. The incorporation of small amounts of transition metals into zeolitic frameworks moderates their properties and generates their redox activity. Zeolites, with their well organized and regular system of pores and cavities, also represent almost ideal matrices for hosting nanosized particles, *e.g.* transition metal oxides, which can also be involved in catalytic applications (Hartman & Kevan,

1999). The second largest group of microporous materials that is known is the aluminophosphate family, members of which were first synthesized in 1978 (Wilson *et al.*, 1982). The aluminophosphate AlPO_4 frameworks are formed from vertex-sharing AlO_4 and PO_4 tetrahedra. The Al/P ratio is usually one making the framework electrostatically neutral with no active sites present. Isomorphous substitution of framework Al or P atoms with divalent transition metals, such as Mn, Co, Fe *etc.*, generates negative framework sites and makes these microporous materials very successful selective catalysts. Many of the structure types are the same as those observed in the zeolite family and there are also new structures known, unique to the aluminophosphates, with ring sizes greater than those found in zeolites. Transition metal modified microporous molecular sieves, with aluminosilicate and aluminophosphate frameworks, catalyse a wide variety of synthetically useful oxidative transformations, using clean oxidants such as hydrogen peroxide or oxygen, under relatively mild conditions (Hartman, 2000). Research has now progressed where new microporous metallophosphates from many elements other than aluminium can be synthesized, such as gallophosphates and other transition metal phosphates. These have differing chemistry and coordination geometry that have led to new structures and new possible applications (Davis, 2002; Szostak, 1998).

The design, synthesis and modification of these materials are challenging and have to be well controlled. Microporous materials are in general prepared hydrothermally from aqueous gels containing a source of the framework-building elements (Al, Si, P, Ga), a mineraliser (OH^- , F^-), regulating the dissolution and condensation processes during the crystallization, and a structure-directing agent (usually an organic amine or ammonium salt). Transition metals can be incorporated into microporous materials by ion exchange (zeolites) (Barrer, 1978), or framework substitution by the addition of transition metal cations to the synthesis gel (for aluminophosphate and gallophosphate systems) (Cheetham *et al.*, 1999).

Elucidation of the structures of these materials is essential for the understanding and prediction of their macroscopic physical and chemical properties; firstly, the size and connectivity of the channels and cavities determine their molecular sieving capability; secondly, the coordination, location, oxidation state and strength of bonding of the divalent and other transition metal ions are directly related to their activity/selectivity in catalytic and other reactions (Cejka, 2002). The conventional single crystal diffraction methods, which normally yield the most complete answers about the structures of ordered crystalline materials, are not always able to provide structural information with sufficient reliability for microporous structures (McCusker, 1991). The first problem is the small size of the crystals that often require *ab initio* powder structure solutions. The second problem is the low concentration and often random distribution of active metal sites over the framework or extra-framework positions that cannot be detected by conventional crystallographic methods. The positions of often disordered template molecules and

template–framework interactions are also difficult to determine, but are necessary for an understanding of the formation of microporous materials.

New strategies and techniques are constantly being developed for the characterization and property evaluation of microporous materials (McCusker, 1991). Rapid development of synchrotron radiation sources has resulted in a tremendous progress in this field of research (Cheetham & Wilkinson, 1992; Harding, 1996; Clegg, 2000). Microcrystallography, harnessing second- and third-generation synchrotron radiation sources, is changing the boundary between ‘single crystal’ and ‘powder’ samples, allowing single crystal precision to be obtained for micrometre- and submicrometre-sized crystals (Cernik *et al.*, 1997; Ohsumi *et al.*, 1991; Broach *et al.*, 1999). A new approach, which is likely to have application to microporous materials, uses simultaneous refinement of individual grains in polycrystalline solids (Schmidt *et al.*, 2003). Moreover, the wavelength tunability of synchrotron radiation can be harnessed for anomalous dispersion methods, which have given new insights into the incorporated transition elements in microporous materials (Helliwell, 2000; Bazin *et al.*, 2002). Another method which can sometimes be used to determine low concentrations of metal atoms in microporous materials is neutron diffraction (Cheetham & Wilkinson, 1992), and this has been applied successfully in the determination of the titanium-substituted sites in Ti silicalite (Henry *et al.*, 2001). Synchrotron radiation has enabled *in situ* diffraction studies, mainly applied to powder samples, of the structural changes during synthesis, crystallization and phase transitions of microporous materials, as a function of temperature or pressure (see for example, Norby & Hanson, 1998, and references therein; Norby *et al.*, 1999; Christensen *et al.*, 1998; review by Walton & O’Hare, 2000; Walton *et al.*, 2002). Also, *in situ* studies of reaction kinetics have been carried out by following the structural changes during the adsorption, removal of the template, catalysis and other processes taking place on microporous surfaces (Ciraolo *et al.*, 2001; Milanesio *et al.*, 2003; Dalconi *et al.*, 2003; Norby & Hanson, 1998; Muncaster *et al.*, 1999). Combined use of XRD and XAFS has been applied to *in situ* studies of microporous materials, monitoring processes involving metal atoms, to chart changes in the metal ion environment, migrations, changes in oxidation state and catalytic processes (Sankar *et al.*, 1994, 1995; Dooryhee *et al.*, 1991; Dent *et al.*, 1995; Thomas & Sankar, 2001).

In this review, we describe the use of softer X-rays in the structure elucidation of microporous materials, firstly by use of anomalous dispersion methods applied to transition metal substituted single crystal samples, secondly, for *ab initio* structure determination of powder samples, and finally, the use of X-ray absorption spectroscopy for the determination of the metal atom environment and oxidation state.

2. Anomalous dispersion of single crystal microporous samples

Although the crystals of microporous materials are generally small and weakly diffracting, when sufficiently large crystals

can be grown, single crystal X-ray diffraction methods generally lead to more precise crystal data than powder diffraction methods (except for lattice parameter determination). This is because reflections, which may overlap in the powder pattern, will be fully resolved using single-crystal methods. Thus, the geometry of the framework and probably the extra-framework template and/or cations should be readily determined. However, active metal atom sites that are substituted into the framework are extremely difficult to locate because they are normally present in low concentration, and they often have similar atomic scattering factors and occupy the same site(s) as the dominant metal atom; when the atomic numbers of the metals are sufficiently different, refining the occupancies can give the degree of substitution at each metal atom site; on the other hand, single wavelength crystallography cannot yield conclusive information about the sites of incorporation of the active metal atom species, when their atomic scattering factors are very similar.

One method of addressing this problem is to use the anomalous dispersion (MAD) technique [reviewed by Helliwell (2000) and by Cheetham & Wilkinson (1992)]; this exploits the large changes in the atomic scattering factor which take place close to the absorption edges of elements, owing to the variation of f' and f'' with wavelength, where the atomic scattering factor is given by

$$f = f_0 + f' + if''.$$

f_0 is the scattering factor of the unperturbed atom and f' and f'' are the real and imaginary components of the anomalous scattering, respectively. At wavelengths remote from atomic absorption edges, the anomalous scattering terms are small and vary slowly, but when the wavelength of the radiation is close to an absorption edge there are large changes in these terms. By altering the atomic scattering factor of the atom in this way, it can be identified and its position in the framework determined. Generally the method involves data collection at a wavelength close to the absorption edge of the element under investigation, and at a wavelength remote from the absorption edge. After appropriate scaling of the data measured at different wavelengths and calculation of a suitable phase set, it is then possible to determine the site(s) of the metal atom, owing to the difference in its f' value at the two wavelengths; this is achieved either by calculation of a difference Fourier map or by refinement of the occupancies. For non-centrosymmetric samples it is also possible to exploit the large increase in f'' close to the absorption edge, which leads to non-equivalence of Friedel pairs of reflections and can allow the calculation of anomalous difference maps, to determine the metal atom positions. Finally, a change of valence state alters the edge position slightly, with an increase of valence state of 1, leading to an increase of the energy of typically 2–6 eV; this phenomenon can be utilized in valence-contrast experiments, which distinguish between valence states of different sites of an element.

We first used this method in a test case to determine the site of a fully occupied Ni atom in the aluminophosphate NiAlPO (Helliwell *et al.*, 1996). Data were collected using synchrotron

Table 1

Peak heights and distances of peaks from the refined Ni atom site for f' difference Fourier maps derived from three wavelength pairs.

	$\Delta f'$ (e)	Peak height (arbitrary units)	Distance from refined Ni atom position (Å)
Mo $K\alpha$, 1.486 Å	7.8	18.0 (7)	0.025
Cu $K\alpha$, 1.486 Å	4.5	13.8 (6)	0.057
Mo $K\alpha$ – Cu $K\alpha$	3.3	6.9 (3)	0.189

radiation at the National Synchrotron Light Source, close to the Ni K -absorption edge, and also at Mo $K\alpha$ and Cu $K\alpha$ wavelengths; this allowed the calculation of various f' difference Fourier maps, exploiting the differences in f' for Ni at the three wavelengths. The results, which are summarized in Table 1, clearly showed that the peak heights and their positional accuracy are a function of the size of $\Delta f'$.

Anomalous dispersion experiments become vital if a sample contains more than one element with similar atomic scattering factors, distributed over several sites in the sample. It then becomes necessary to collect multiple data sets at different wavelengths, close to the absorption edges of each element in turn, together with a reference data set at a wavelength removed from all of the absorption edges. Such methods have been used, for example, to determine the site occupancies of Ni, Mn, Al and Co over two sites in the battery electrode material $\text{LaNi}_{3.55}\text{Mn}_{0.4}\text{Al}_{0.3}\text{Co}_{0.75}$ in a multiple-wavelength powder diffraction experiment (Joubert *et al.*, 1998). Other examples are reviewed by Helliwell (2000) and Cheetham & Wilkinson (1992). We have used such techniques applied to single crystal samples to determine metal atom incorporation in a cobalt containing zincophosphate and three zinc gallium phosphates, and these results are outlined below.

The first study was to determine the site of Co incorporation in the zincophosphate CoZnPO-CZP in a five wavelength experiment (Helliwell *et al.*, 1999); CoZnPO-CZP is a phosphate-based molecular sieve, forming chiral hexagonal crystals (space group $P6_522$ or $P6_122$), with Co substituted to an extent of about 20% over the two independent metal atom positions; Cu $K\alpha$ data collected on a rotating anode diffractometer were used for the structure solution and refinement but, owing to the lack of scattering contrast between Co and Zn, the distribution of Co over the two metal atom sites could not be unambiguously determined. In order to resolve this, synchrotron radiation data were collected at ELETTRA at the f' minimum and f'' maximum for both Co and Zn, and also at a wavelength remote from the K absorption edges of either of the metal atoms (at 1.45 Å), using a MAR image plate. Co and Zn f' difference Fourier maps were then calculated, which clearly showed that there was a high proportion of Zn at each site (as expected), and that the Co atom incorporation occurred mainly at the metal 1 site.

Recently, Cowley *et al.* (2002) distinguished isoelectronic zinc and gallium cations in the framework of three zinc gallium phosphates (ZnGaPOs) using multiple-wavelength MAD methods and synchrotron radiation data measured on station 9.8 at the SRS, Daresbury. Crystals of the three materials were

Table 2Values of f' and f'' for Zn and Ga at the Zn and Zr K edges.

	Zn edge radiation	Zr edge radiation
Wavelength (Å)	1.2857	0.6912
Anomalous scattering	$f' = -6.147$	$f' = 0.214$
corrections for Zn (e)	$f'' = 0.488$	$f'' = 1.367$
Anomalous scattering	$f' = -2.367$	$f' = 0.162$
corrections for Ga (e)	$f'' = 0.599$	$f'' = 1.538$

prepared by solvothermal methods from gel precursors to give $(\text{C}_7\text{H}_{14}\text{N})[\text{ZnGa}_3(\text{PO}_4)_4]$ (I), $(\text{C}_5\text{H}_6\text{N})[\text{ZnGa}_2(\text{PO}_4)_3]$ (II) and $(\text{C}_6\text{H}_{14}\text{N}_2)_2[\text{Zn}_4\text{Ga}_5(\text{PO}_4)_9]$ (III). These materials have frameworks constructed from alternating PO_4 and MO_4 ($M = \text{Zn}$ and Ga) tetrahedra with CGS, LAU and CGF (Baerlocher *et al.*, 2001) topologies, respectively. Data were collected close to the Zn K absorption edge (~ 1.29 Å) and at a wavelength remote from the Zn or Ga K edges, close to the Zr $K\alpha$ edge at about 0.7 Å (to be near to the Mo $K\alpha$ wavelength), for each sample; the values of f' and f'' at each wavelength are shown in Table 2. Initial refinement of the coordinates and atomic displacement parameters (adps) was carried out using the zirconium K edge data. Then, using the zinc K edge data, the site occupancies of the metal atom sites were refined such that the total occupancy was constrained to sum to unity, but with no restraint on the overall Zn:Ga ratio. This cycle of refinement, using the Zr and Zn K edge data sets alternately to refine the coordinates and adps, then the occupancies, respectively, was repeated until convergence of the parameters was reached. Table 3 shows the final parameters for the four metal atom sites in I, three metal atom sites in II, and five metal atom sites in III. The refined occupancies were determined to a high degree of accuracy; for II and III, the framework composition is close to that required to balance the charge of the template; for I, the agreement is not so close, but the composition of this material is known to be variable.

One question which is important in assessing the viability of this method for locating partially occupied metal atoms, substituted into a microporous framework, is how low can the metal concentration be? Generally, data collection at the f' minimum for the K edge of a first row transition element induces a change in f' of 6 to 10 electrons, with respect to the reference wavelength, and this will change the amplitudes by an extent given by the average dispersive amplitude difference, DD,

$$\langle F_{\lambda E} - F_{\lambda R} \rangle / \langle F_{\lambda R} \rangle = \text{DD} = (N_A/N)^{1/2} \Delta f' / f_0 \quad (1)$$

where $F_{\lambda E}$ and $F_{\lambda R}$ are the structure factor amplitudes of the absorption-edge data and reference data, respectively, N_A is the number of atoms which are anomalous scatterers, N is the number of non-anomalous scattering atoms, $\Delta f'$ is the difference in f' for the anomalous scatterer between the two wavelengths, and f_0 is the average atomic scattering factor [Helliwell (1992), based on Crick & Magdoff (1956)].

Similarly, the average anomalous difference of the amplitudes between Friedel pairs of reflections for a chiral sample is given by

Table 3

Refined site occupancies of the metal atom sites for (a) I, (b) II and (c) III.

Atom	Occupancy	Atom	Occupancy
(a)		(c)	
Ga1	0.50 (1)	Ga1	0.723 (9)
Ga2	0.74 (1)	Ga2	0.719 (8)
Ga3	0.75 (1)	Ga3	0.43 (1)
Ga4	0.67 (1)	Ga4	0.089 (9)
Zn1	0.50 (1)	Ga5	0.688 (9)
Zn2	0.26 (1)	Zn1	0.277 (9)
Zn3	0.25 (1)	Zn2	0.281 (8)
Zn4	0.33 (1)	Zn3	0.57 (1)
		Zn4	0.911 (9)
(b)		Zn5	0.312 (9)
Ga1	0.699 (12)		
Ga2	0.610 (12)		
Ga3	0.612 (12)		
Zn1	0.301 (12)		
Zn2	0.390 (12)		
Zn3	0.388 (12)		

$$\langle F_{\lambda P}^+ - F_{\lambda P}^- \rangle / \langle F_{\lambda R} \rangle = \text{AD} = 2^{1/2} (N_A/N)^{1/2} \Delta f'' / f_0 \quad (2)$$

where $F_{\lambda P}^+$ and $F_{\lambda P}^-$ are the hkl and $\bar{h}\bar{k}\bar{l}$ amplitudes of the data measured at the f'' maximum, and f'' is the value of f'' for the anomalous scatterer, at the wavelength of the data collection (Olczak *et al.*, 2003).

For CoZnPO-CZP and the three zinc gallium phosphates there are two anomalous scatterers and so there is a contribution to the dispersive difference from both metal atoms A and B , giving rise to a total dispersive difference equal to $(\text{DD}_A^2 + \text{DD}_B^2)^{1/2}$. For each case, the component DDs are calculated here by assuming that the proportion of each metal atom at all sites is that given by the formula; for example, for $(\text{C}_7\text{H}_{14}\text{N})[\text{ZnGa}_3(\text{PO}_4)_4]$ it is assumed that each of the four metal atom sites contains 0.25 Zn and 0.75 Ga. Similarly, there is a contribution to the AD from both Co and Zn, for CoZnPO-CZP, which is the only chiral sample, and here the total AD is given by $(\text{AD}_{\text{Co}}^2 + \text{AD}_{\text{Zn}}^2 + \text{AD}_{\text{CoZn}})^{1/2}$, *i.e.* there is a cross-term contribution to the AD (Olczak *et al.*, 2003). Table 4 shows the component DDs for the contributing elements for all the above microporous samples, and the ADs for the chiral case, CoZnPO-CZP.

In all the experiments, the DD was sufficiently large, in practice, to locate and determine occupancies for the substituted metal atoms. In the case of CoZnPO-CZP, where the Co:Zn ratio was 0.2:0.8, it was important to collect data as close as possible to the f' dip of cobalt, maximizing the signal, which allowed the successful detection of its distribution over the two available sites. For $(\text{C}_7\text{H}_{14}\text{N})[\text{ZnGa}_3(\text{PO}_4)_4]$, I, the DD for Ga is in fact larger than that of Zn, which could in part explain why the refined values were not as close to the expected values as for compounds II and III, where the Zn proportions were higher; another factor is that I is known to show variable composition (see above). The anomalous signal at the Co f'' maximum did not yield significant results for the Co incorporation in CoZnPO-CZP, and it is clear from the small and similar ADs for Co and Zn that this is to be expected. The results for the determination of Zn at the f'' maximum for Zn were also not conclusive, although the two

Table 4

Values of $\Delta f'$, f'' , as well as the dispersive and the anomalous differences (for CoZnPO-CZP), calculated using equations (1) and (2), respectively, are given for each compound at various K -absorption edges.

Sample	K -absorption edge	$\Delta f'$ (e)	Dispersive difference (%)	f'' (e)	Anomalous difference
NiAPO: NiAl ₃ P ₄ O ₁₈ C ₄ H ₂₁ N ₄	Ni	7.8	14.3	0.48	–
CoZnPO-CZP: Na ₆ [Co _{0.2} Zn _{0.8} PO ₄] ₆ ·6H ₂ O	Co	$\Delta f'_{Zn} = 0.5$ $\Delta f'_{Co} = 10.0$	1.2 6.4	$f''_{Zn} = 0.7$ $f''_{Co} = 3.9$	2.6 3.5
CoZnPO-CZP: Na ₆ [Co _{0.2} Zn _{0.8} PO ₄] ₆ ·6H ₂ O	Zn	$\Delta f'_{Zn} = 9.7$ $\Delta f'_{Co} = 1.0$	24.6 0.6	$f''_{Zn} = 3.9$ $f''_{Co} = 2.7$	14.0 2.4
(C ₇ H ₁₄ N)[ZnGa ₃ (PO ₄) ₄]	Zn	$\Delta f'_{Zn} = 5.9$ $\Delta f'_{Ga} = 2.2$	5.0 5.5	$f''_{Zn} = 0.49$ $f''_{Ga} = 0.60$	–
(C ₅ H ₆ N)[ZnGa ₂ (PO ₄) ₃]	Zn	$\Delta f'_{Zn} = 5.9$ $\Delta f'_{Ga} = 2.2$	6.6 4.9	$f''_{Zn} = 0.49$ $f''_{Ga} = 0.60$	–
(C ₆ H ₁₄ N ₂) ₂ [Zn ₄ Ga ₅ (PO ₄) ₉]	Zn	$\Delta f'_{Zn} = 5.9$ $\Delta f'_{Ga} = 2.2$	8.7 4.1	$f''_{Zn} = 0.49$ $f''_{Ga} = 0.60$	–

largest peaks in the anomalous difference Fourier map for the zinc are reasonably close to the expected positions; the lack of a clear result is presumably because the data sets were of limited resolution, and therefore the number of Friedel pairs of reflections was small; in the case of the Zn K edge data, where the resolution limit was 1.44 Å using the fixed MAR image plate, there were 42 such pairs of reflections, while for the Co edge data, where the resolution limit was 1.80 Å, there were only 19 Friedel pairs.

As a quantitative assessment of general applicability, we can derive an expression for the DD of a typical phosphate-based microporous material, $M'_n M_m (\text{PO}_4)_{m+n} T_n$, using equation (1) [where M' is the incorporated metal 2^+ ion, M is the metal 3^+ ion (Al, Ga *etc.*) and T is the template cation], assuming that M' is distributed over all the $m+n$ metal atom sites; then the number of anomalous scatterers, $N_A = m+n$, the number of light atoms, N , is $(\text{PO}_4)_{m+n} T_n$, *i.e.* $[5(m+n) + Tn]$, and the proportion of M' at each site is $n/(m+n)$,

$$\text{DD} = \left[\frac{m+n}{5(m+n) + Tn} \right]^{1/2} \frac{n \Delta f'}{(m+n) f_0}. \quad (3)$$

Squaring and rearranging (3) gives

$$n^2 \left[\left(\frac{\Delta f'}{f_0 \text{DD}} \right)^2 - T - 5 \right] - n(10m + Tm) - 5m^2 = 0. \quad (4)$$

By analogy with MAD results from protein crystallography, we should be able to detect a signal in terms of a measurable change in the diffraction amplitudes if the DD is greater than 3%. Generally, f_0 is on average between 10 and 12 electrons for microporous materials (close to 10 electrons for zeolites and aluminophosphates, and between 11 and 12 electrons for gallophosphates and zincophosphates), and if we assume that the template molecule has six atoms it is then possible to compute the maximum m/n fraction for a particular value of $\Delta f'$, that will lead to a measurable signal, using (4). The results for f_0 values of 10 and 12 electrons are plotted in Fig. 1. (Note that the m/n value is fairly insensitive to the number of T atoms, varying from 12.8 for $T = 10$ to 13.9 for $T = 0$, assuming that $\Delta f'$ and f_0 are both 10 electrons.) Thus, from Fig. 1, one anomalous scatterer distributed over between 11 and 13 metal atom sites will give a measurable change in intensity, if one can

induce a $\Delta f'$ of 10 electrons, between the reference and absorption edge data sets. This would be equivalent to less than one electron per site, which would be difficult to 'see' by either difference Fourier techniques, or by refinement of the occupancies. Thus, one might realistically expect to be able to locate a single anomalous scatterer distributed over half the maximum number of sites.

Similar estimations can be made for metal-substituted zeolites and related materials that already have a negatively charged framework that is balanced by means of extra-framework alkali or alkaline earth metal counterions. A typical formula might be $M'_n M_m (\text{ASO}_4)_{m+n}$, where M' is the substituted metal atom, M is the dominant metal atom (*e.g.* Al, Zn), A is an alkali metal and S is a tetrahedral atom such as Si or P; here, no account is taken of additional extra-framework species, such as water molecules or other templates, or that the valence state of M' may be different from that of M . For this general chemical formula, and assuming that M' is distributed over all the $m+n$ framework metal atom sites, it can readily be shown that

$$m/n = \Delta f' / (\sqrt{6} f_0 \text{DD}) - 1 \quad (5)$$

and now the maximum m/n value (assuming $f_0 = 10$ electrons, DD = 3% and $\Delta f' = 10$ electrons) is 12.6 atoms, in line with results obtained above using (4).

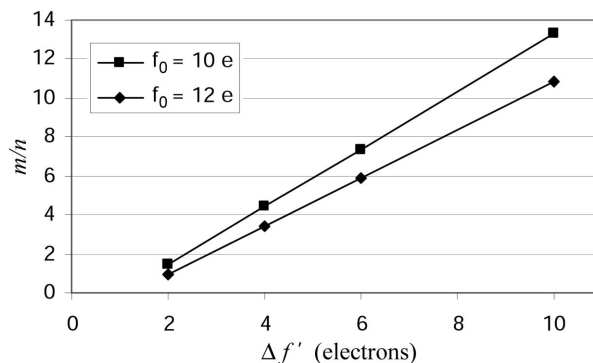


Figure 1
Plot of maximum m/n values versus $\Delta f'$ calculated using equation (4) for $f_0 = 10$ and 12 electrons. A dispersive difference of 3% and six template atoms are assumed.

Matters improve considerably if the anomalous scatterer, M' , at occupancy n , is located on just one of the metal atom sites; then for the typical phosphate-based microporous material, $M'_n M_m (\text{PO}_4)_{m+n} T_n$, $N_A = 1$, $N = [5(m+n) + (m+n) + Tn - 1]$, so

$$\text{DD} = \{1/[6(m+n) + Tn - 1]\}^{1/2} n \Delta f' / f_0 \quad (6)$$

$$m = (1/6) \left\{ [(n \Delta f') / (f_0 \text{DD})]^2 - Tn - 6n + 1 \right\}. \quad (7)$$

Thus for a particular occupancy, the maximum m (again assuming $\text{DD} = 3\%$ is enough to induce a measurable signal) is proportional to $\Delta f'^2$, so that it becomes particularly important to maximize the value of $\Delta f'$. Fig. 2 shows the derived values of m plotted against $\Delta f'$ (assuming $f_0 = 10$ electrons and $T = 6$) for various occupancies of M' substituted at one site only. There is also one example where the 0.5 atoms of M' are substituted over two sites; this shows the impact of distributing 0.5 atoms over two sites compared with just one, very much reducing the maximum value of m . For an occupancy of $n = 1.0$, the maximum m is 183 atoms, and the formula of the microporous sample could in theory be $M' M_{183} (\text{PO}_4)_{184} T$. Thus, it should be possible to locate one fully occupied anomalous scatterer in more than 1000 atoms of a microporous sample if the $\Delta f'$ value is 10 electrons. This compares well with the case of a single fully occupied anomalous scatterer in a protein, which can be detected among 2000 light atoms (Einspahr *et al.*, 1985).

It becomes more difficult to generalize when there is more than one anomalous scatterer contained in a microporous sample; then, not only are the occupancies of each metal at the different sites important, but so also is the proximity of the absorption edges of the respective elements to one another. When the absorption edges are reasonably far apart, then the dominant metal atom does not mask the signal of M' , as seen in the case of CoZnPO-CZP (see Table 4). On the other hand, for adjacent metals in the periodic table, such as in the case of zinc gallium phosphates, the absorption edges are so close together that there is a significant signal from the dominant metal atom, M . As a rule, by using equations (4) or (5), it can

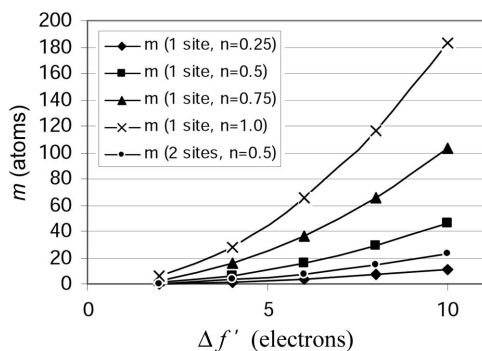


Figure 2
Plot of maximum m for a dispersive difference of 3% versus $\Delta f'$ calculated using equation (7) for various occupancies n of M' . It is assumed that M' is substituted at one, or in one case, over two sites, and that $f_0 = 10$ electrons and the number of template atoms is 6.

be shown that, for a sample containing two anomalous scatterers,

$$\text{DD}_{M'}/\text{DD}_M = n \Delta f'_M / m \Delta f'_M. \quad (8)$$

Using this equation it is possible to compute the ratio of DDs for M' to M for a sample of known composition using values of $\Delta f'$ for the two metal atom types at a particular wavelength. If the $\text{DD}_{M'}/\text{DD}_M$ ratio is close to or less than 1, then the signal from M' starts becoming masked by that of M , and in order to detect M' it may then be necessary to measure data at a number of wavelengths around the absorption edge of M' , to vary its $\Delta f'$, while that of M remains approximately constant.

Overall, optimization of the detector provision is essential, particularly for elements whose absorption edges are at long wavelengths, *i.e.* where the resolution limit of the data may limit the scope of this method and thus reduce the lower limit of the detectable metal. However, CoZnPO-CZP experiments show that site-specific identification was successful down to a resolution limit of 1.8 Å. Thus if full backscattering were available, the wavelength coverage could even be up to 3.6 Å, therefore including the calcium K edge at 3.07 Å. In addition, to obtain maximum sensitivity, particularly where two anomalous scatterers are present, it is necessary to tune as close to the f' dip or f'' maximum as possible to provide optimal contrast between the signals from the two elements. This requires tailored instrumentation to allow fine $\delta\lambda/\lambda$ selection, straightforward wavelength tuning, and wavelength stability (especially for data collection at the f' dip and f'' maximum). These needs are the same as for MAD protein crystallography (see, for example, Cassetta *et al.*, 1999), but the resolution coverage for MAD small molecule crystallography is more demanding. In addition, the use of experimentally determined values of f' and f'' from the X-ray spectra of representative model compounds would enhance the accuracy of this approach (Evans & Pettifer, 2001). Account of these requirements will be important for new small molecule beamlines, such as that planned at Diamond (www.diamond.ac.uk).

3. Powder diffraction using softer X-rays

Often, when single crystals of sufficient size of microporous materials cannot be grown, powder diffraction techniques are required, with the accompanying difficulties of *ab initio* structure solution from powder samples, particularly for larger structures (McCusker, 1991; David *et al.*, 2002). However, there has been rapid growth of structures that have been determined *ab initio* by powder diffraction, with the number now standing in excess of 600 (Le Bail, <http://sdpd.univ-lemans.fr/postscript/ecm18.pdf>). This is in part due to the use of synchrotron radiation sources, with their superior instrumental resolution and signal-to-noise ratio (Cernik *et al.*, 1990). The initial proof of concept experiment in which the anti-ulcer drug cimetidine was determined (Cernik *et al.*, 1991) used a pseudo single crystal approach in which the pattern was decomposed to give individual structure factor amplitudes, and then structure solution was achieved using direct methods

(Burla *et al.*, 1989). There are several problems with this two-step approach, which are a consequence of the overlap of reflections, leading to an incorrect estimation of the intensity values. This causes problems at the initial normalization stage during conventional direct methods, when the E values used in subsequent calculations are produced. These incorrect E values can lead to problems in the misassignment of the space group, *e.g.* centrosymmetric *versus* non-centrosymmetric, but more crucially in the production of structure invariants which lie at the heart of a direct methods approach. Much of the effort since this time has been devoted to developing alternative routes to the solution of structures from powder data, *e.g.* Monte Carlo methods (Harris *et al.*, 1994; Tremayne *et al.*, 1997), simulated annealing (David *et al.*, 1998) and genetic algorithms (Shankland, David & Csoka, 1997; Kariuki *et al.*, 1997). In the area of microporous solids, a notable addition to the available methods was the development of the FOCUS method (Grosse-Kunstleve *et al.*, 1997), which makes use of both the occurrence of the three-dimensional network structure of such materials and the fact that the tetrahedral sites are f -connected. This, coupled with an automatic Fourier recycling routine, had been used to solve the structures of both known (Grosse-Kunstleve *et al.*, 1997) and unknown materials (Burton & Elomari, 2004). There has also been interest in improved methodologies of data collection. One approach is to exploit the anisotropic thermal expansion of solids, which can be used to resolve partially overlapping reflections (Shankland, David & Sivia, 1997); a recent elegant use of this technique was presented by Brunelli *et al.* (2003). Despite these advances, structure solution from powder data is still not routine compared with single crystal structure determination of equally complex structures (Le Bail, <http://sdpd.univ-lemans.fr/postscript/ecm18.pdf>).

One area that has been little exploited is the use of synchrotron radiation of a longer wavelength, although there are potential problems such as absorption by the air and by the capillary (if used). The principal advantage of using a longer wavelength is straightforward in that for a given angular range in 2θ there are fewer reflections; hence overlap between peaks is diminished and decomposition of a powder pattern prior to a pseudo single crystal structure solution is simplified. Provided that data are collected to sufficient resolution, which in practical terms corresponds to 1.0–1.2 Å, it is still possible to use direct methods. This approach was adopted in the structure solution of an open framework zinc phosphate DAF-3 (Jones *et al.*, 1994). This compound was obtained using a gel formed from zinc oxide and phosphoric acid with ethylene diamine as the template, at room temperature. Data were collected in flat-plate mode at station 2.3, SRS Daresbury Laboratory, using a wavelength of 1.72984 Å. Following indexing of the pattern (Visser, 1969), a tetragonal cell was obtained and the systematic absences suggested that the space group was either $P4_2bc$ or $P4_2/mbc$. Using the space group $P4_2bc$, individual reflections were extracted (Murray *et al.*, 1990) to yield 437 reflections, which were input into a direct methods program (Sheldrick, 1985). From a trial solution it was possible to locate four heavy

atoms, corresponding to two Zn and two P atoms, in the asymmetric unit. Using the extracted reflections and Fourier techniques it was possible to further develop the model to give the complete structure and template molecules. This model was then refined by Rietveld methods (Peter *et al.*, 1996) with constraints applied to the interatomic distances to give final residuals of $R_{wp} = 0.22$ and $R_I = 0.11$. Despite the relatively large residuals, the topology of the framework is almost certainly correct.

The main drawback of collecting data with a longer wavelength is immediately discernable in the previous example. While solving the structure may prove tractable, it is sometimes difficult to obtain accurately refined structural parameters owing to a limited data-to-parameter ratio and possible problems with absorption. In the previous example, data were only collected to $144^\circ 2\theta$, leading to a total of 537 unique reflections for a structure containing 16 non-H atoms. A more useful approach would be to solve the structure with longer wavelength data, but recollect data at a shorter wavelength for the refinement. This strategy was successfully employed in determining the structure of the layered titanosilicate JDL-L1 (Roberts *et al.*, 1996). The structure was initially solved using data collected in flat-plate mode with $\lambda = 1.59939$ Å, again using a pseudo single crystal approach. However, because of the layered nature of the material which causes the sample to suffer from preferred orientation, and the limited data set, it was necessary to also collect data in capillary mode using X-rays of a shorter wavelength ($\lambda = 1.20000$ Å). The data at a higher resolution enabled an excellent structural model to be developed ($R_I = 0.073$, $R_{wp} = 0.169$) with no necessity to make recourse to restraints. The validity of the model was also confirmed by an EXAFS study on the material. From these two studies, good agreement was obtained for the interatomic contacts derived from X-ray diffraction measurements and those found by EXAFS (indicated in parentheses): Ti–O 1.707 (5) Å (1.70 Å); Ti–O 1.946 (3) Å (1.96 Å); Ti–Si 3.350 (1) Å (3.37 Å); and Ti–Na 3.7305 (4) Å (3.68 Å).

These structures were determined prior to the major advances in computational methodology which were outlined earlier in the powder diffraction section. Thus the potential of the softer X-ray powder diffraction method has not yet been fully developed and promises the determination of even more complicated structures from powder data.

4. X-ray absorption spectroscopy

In some cases, when crystals or powders of investigated materials are not suitable for anomalous diffraction methods, X-ray absorption spectroscopy provides excellent information on short-range order for selected atomic species in terms of the number of neighbours, distances and thermal and static disorder within the range of those distances. EXAFS (extended X-ray absorption fine structure) and XANES (X-ray absorption near-edge structure) have been successfully used in the structure analysis of several microporous structures (Barrett *et al.*, 1996). Our recent work in X-ray absorption spectroscopic analysis was concentrated on

manganese-, iron-, titanium- and cobalt-modified silicates and aluminophosphates (Arcon *et al.*, 1999; Tuel *et al.*, 1996; Novak Tusar *et al.*, 2001, 2002, 2003; Ristic *et al.*, 2003).

4.1. Mn silicalite-1

Silicalite-1 is a microporous silica-based molecular sieve with a MFI topology possessing channels of diameter 5.5 Å (Baerlocher *et al.*, 2001). The isomorphous substitution of Si⁴⁺ ions in silicalite-1 with trivalent ions such as Al³⁺, B³⁺, Fe³⁺ and Ge³⁺ has been reported to result in high-quality inorganic membranes used for catalytic membrane reactors. Manganese-containing silicalite-1 (MnS-1) (Round *et al.*, 1997; Ko *et al.*, 1999) was synthesized hydrothermally using the structure-directing agent (template) tetraethylammonium hydroxide for the first time; the template-free MnS-1 was prepared by calcination at 823 K in an oxygen flow. The incorporation of manganese into the framework sites of silicalite-1 was shown by elemental, thermogravimetric and cation exchange analyses. The reasons that a detailed X-ray diffraction study of the Mn incorporation could not be carried out were, firstly, the complexity of the MFI topology with a large unit cell and 12 crystallographically different silicon sites that might be randomly occupied with a very low amount of manganese (0.5% isomorphous substitution of silicon by manganese), and, secondly, the small size of crystals in the final product (only up to 5 µm), although, as described in the *Introduction*, such samples may be tractable by employing intense synchrotron radiation sources; however, using the X-ray absorption spectroscopic methods XANES and EXAFS we were able to confirm the incorporation of Mn³⁺ into the silicalite-1 framework.

X-ray absorption spectra of the template-free MnS-1 and reference samples in the energy region of the Mn *K* edge were measured at beamline E4 of HASYLAB synchrotron facility

at DESY in Hamburg. Detailed experimental conditions are reported elsewhere (Novak Tusar *et al.*, 2003). The average oxidation number of manganese cations in the template-free MnS-1 sample was deduced from the energy shift of the manganese absorption edge. A linear relation between the edge shift and the oxidation state was established for the atoms with the same type of ligands. For Mn atoms coordinated to O atoms, a shift of 3.5 eV per oxidation state was found (Ressler *et al.*, 1999).

Fig. 3 shows the derivative of absorption of the Mn *K* edge profile of the template-free MnS-1 and reference manganese compounds with known oxidation numbers {Mn²⁺O, K₃[Mn³⁺(C₂O₄)₃].3H₂O and Mn⁴⁺O₂}. The zero energy was taken at the first inflection point of the Mn *K* edge in the spectrum of Mn metal (6539.0 eV), *i.e.* at the 1 s ionization threshold in Mn metal. The precise energy position of the edge was taken at the edge inflection point, which can best be determined in the derivative spectrum as the tip of the first peak. A comparison with reference spectra shows that the edge shift in MnS-1 is the same as in K₃[Mn³⁺(C₂O₄)₃].3H₂O, indicating that the average oxidation state of manganese in MnS-1 is 3+. It is worth noting that the presence of a smaller fraction of Mn²⁺ cations in the sample is not excluded, since the sensitivity of the method in determining the Mn²⁺:Mn³⁺ ratio is about 10%.

The Mn *K* edge EXAFS spectrum of the template-free MnS-1 sample was quantitatively analysed for the coordination number, distance and Debye–Waller factor of the nearest coordination shells of neighbour atoms. A Fourier-transformed *k*³-weighted Mn EXAFS spectrum calculated in the *k* range 5–12 Å⁻¹ is shown in Fig. 4 together with a best-fit EXAFS model. A very good fit in the radial distance (*R*) range from 1.2 to 3.5 Å was found with three O atoms in the first coordination shell, two of them at a shorter distance of 1.93(σ) Å and one at a longer distance of 2.15(σ) Å. In the

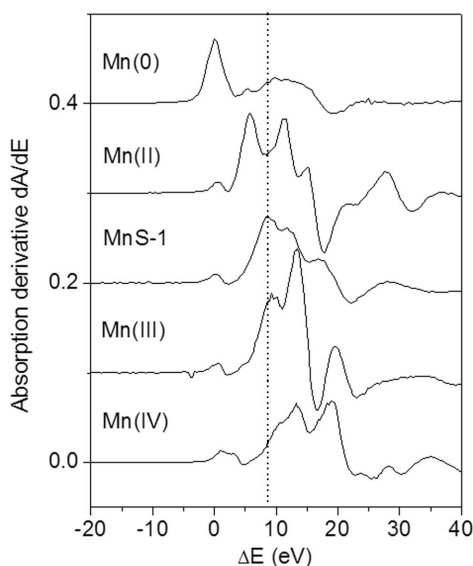


Figure 3 Absorption derivative of the Mn *K* edge profile of the template-free MnS-1 and reference samples. The vertical dashed line is plotted at the energy position of the Mn *K* edge in the MnS-1 spectrum.

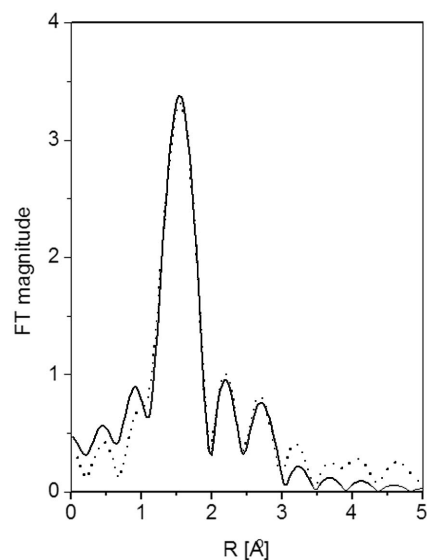


Figure 4 Fourier transforms of the *k*³-weighted Mn EXAFS spectrum of the template-free MnS-1, calculated in the *k* range 5–12 Å⁻¹ (solid line, experiment; dotted line, EXAFS model).

second coordination shell, two O atoms were found at $2.81(\sigma)$ Å and $3.04(\sigma)$ Å. Additionally, at a larger distance of about $3.5(\sigma)$ Å, the presence of Si atoms is indicated, but the weak signal of that neighbour shell is obscured by the noise and the parameters could not be reliably determined. These results of XANES and EXAFS analyses suggest that Mn^{3+} is coordinated by three lattice O atoms in a distorted and coordinatively unsaturated three-fold symmetry, which is characteristic of Lewis acid sites.

4.2. Fe-substituted aluminophosphate FAPO-36

Great care was needed for the synthesis of pure iron-substituted aluminophosphate FAPO-36, which is built from a one-dimensional system of channels, with pores apertures of $7.4 \text{ \AA} \times 6.5 \text{ \AA}$ (Baerlocher *et al.*, 2001). Pure and crystalline FAPO-36 was prepared hydrothermally at 398 K for four days with tripropylamine as structure directing agent (Ristic *et al.*, 2003). Elemental analysis (1% isomorphous substitution of aluminium by iron) and thermogravimetry indicated isomorphous aluminium substitution by iron. X-ray absorption techniques were used to confirm the incorporation of iron into the framework of AlPO_4 -36 and also to establish the redox properties, which are expected to appear with the incorporation of the transition metal (Fe) into the aluminophosphate framework. Therefore we studied the changes in the oxidation state and local structure of the framework iron in the as-synthesized and template-free FAPO-36 materials. The results, which were also supported by the *in situ* IR measurements of CO adsorption, show that changes do occur and that this material could act as redox catalyst.

X-ray absorption spectra in the energy region of the Fe *K* edge were measured in the transmission mode at beamline E4 of HASYLAB synchrotron facility at DESY in Hamburg, using methods similar to those used for MnS-1 (Ristic *et al.*, 2003). The normalized Fe XANES spectra of the samples and reference compounds are shown in Fig. 5. The shape of the *K* edge and the pre-edge show characteristic tetrahedral resonances in both the as-synthesized and template-free FAPO-36, demonstrating that iron cations are incorporated into the tetrahedral sites. The pre-edge peak is weaker in the case of the as-synthesized sample which indicates that the tetrahedral symmetry of the iron cations in this sample is slightly distorted. A linear relation between the edge shift and the valence state changes during calcination was established for the atoms with the same type of ligands. From the spectra of the reference samples (FeSO_4 and FePO_4) with known iron oxidation states we found that the Fe *K*-edge shifts for 3.0 eV per valence state. The Fe XANES spectra of the FAPO-36 samples clearly indicate oxidation of iron cations after the calcination: the Fe *K* edge in the template-free sample is shifted by 1.5 eV to higher energies compared with the as-synthesized sample. From the energy shifts of the Fe *K* edge we obtained an average iron valence of 2.5 ± 0.1 in the as-synthesized and 3.0 ± 0.1 in the template-free sample. We thus conclude that the as-synthesized FAPO-36 contains a mixture

of Fe(II) and Fe(III) in the ratio 1:1, while calcination oxidizes all the Fe(II) in the sample to Fe(III).

The Fe *K* edge EXAFS spectra were quantitatively analyzed for the coordination number, distance and Debye–Waller factor of the nearest coordination shells of neighbour atoms, as for MnS-1. Fourier transform magnitudes of Fe EXAFS spectra are shown in Fig. 6. The fit of the iron first coordination shell was performed in the *R* range from 1.2 Å to 2.3 Å and shows that in the as-synthesized sample iron is coordinated to four O atoms at $1.94(\sigma)$ Å, which indicates the insertion of iron cations into the tetrahedral sites of the as-synthesized FAPO-36 structure. In addition, we found two O atoms at a much longer distance of 2.49 Å with much larger σ^2 value, which indicates that they belong to coordinated water molecules in the pores. In the template-free sample we found four oxygen neighbours at a shorter distances of $1.86(\sigma)$ Å, in agreement with previously reported values for tetrahedrally coordinated Fe(III) cations. There was, however, no evidence for the oxygen neighbours at the longer Fe–O distance, which means that there are no water molecules in the pores coordinated to iron cations. This is in agreement with the structure modification of the template-free sample after the evacuation, when water molecules are removed. Taking into account the XANES results, we can conclude that in the template-free sample, iron is incorporated into the tetrahedral framework sites in the form of Fe(III).

The above EXAFS and XANES studies show how softer X-rays have been applied in the structural studies of microporous materials. Even longer wavelengths have been pioneered in the study of compounds with sulfur and chlorine

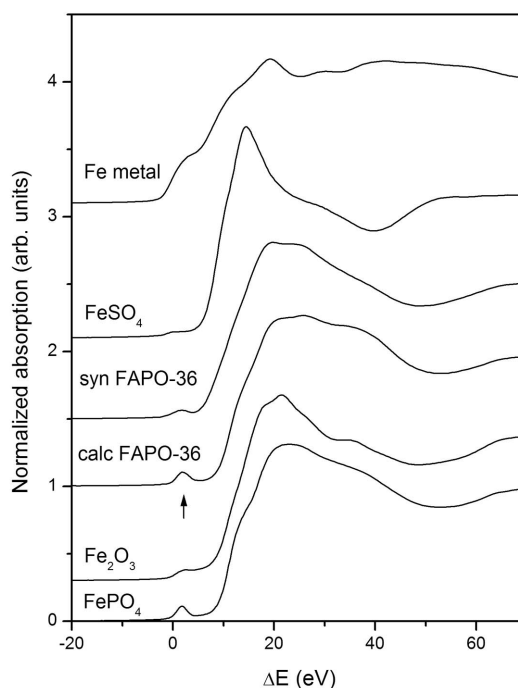


Figure 5
Normalized Fe *K* edge XANES spectra of the as-synthesized and template-free FAPO-36 and references: FePO_4 , FeSO_4 , Fe_2O_3 and Fe metal.

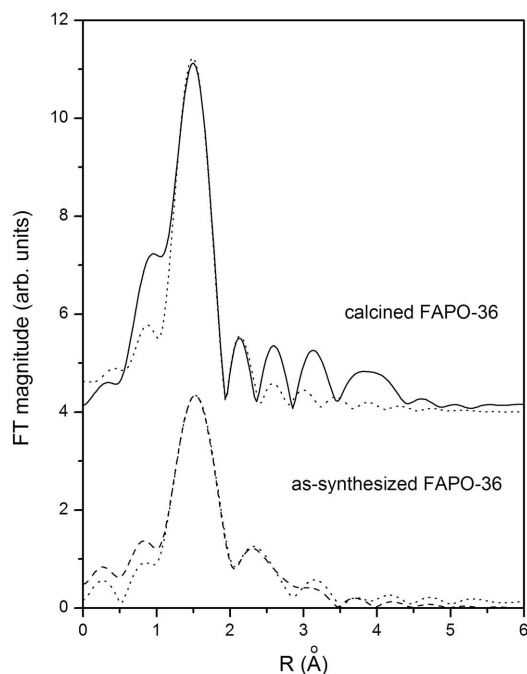


Figure 6

Fourier transforms of k^3 -weighted EXAFS spectra of the as-synthesized and template-free FAPO-36 (experiment, solid line; EXAFS model, dotted line).

containing ligands, where the S and Cl K edges are at 5.0 and 4.4 Å, respectively (see review by Glaser *et al.*, 2000).

5. Conclusions and future developments

Softer X-rays than those traditionally used by structural chemists (*i.e.* Mo $K\alpha$ and Cu $K\alpha$ wavelengths) have a key role to play in the study of microporous solids. Since metal atoms substituted into framework structures must not differ too greatly in size from that of the host elements, their atomic numbers are generally less than that of copper. Consequently, the absorption edges (with the exception of nickel) all lie at wavelengths longer than that of Cu $K\alpha$ radiation. It is also the case that these transition metals are the most important catalytically, by virtue of a range of readily accessible oxidation states. The work described in this review has concentrated on the use of K absorption edges, for studying metal substituted microporous materials by anomalous dispersion single crystal methods and X-ray absorption spectroscopy. However, studies have also been made involving the use of L edges (Berry *et al.*, 1993) on cerium containing zeolites. For *ab initio* structure solution of powder samples, softer X-rays have also proved valuable by spreading out the diffraction pattern and thereby extending the size of the unit cell which can be studied. In diffraction experiments, the limitation lies in suitable experimental configurations to measure higher angle data than usual, in order to obtain the resolution which can be compromised by the use of longer wavelength radiation. However, softer X-rays can be used in a complementary manner to harder X-rays, probing those areas of structural

chemistry of microporous solids which are not easily accessed by conventional X-ray sources or shorter wavelength synchrotron radiation beams.

References

- Arçon, I., Rajic, N. & Kodre, A. (1999). *J. Synchrotron Rad.* **6**, 460–462.
- Baerlocher, Ch., Meier, W. M. & Olson, D. H. (2001). *Atlas of Zeolite Framework Types*. Amsterdam: Elsevier.
- Barrer, R. M. (1978). *Zeolites and Clay Minerals as Sorbents and Molecular Sieves*. London: Academic Press.
- Barrett, P. A., Sankar, G., Catlow, C. R. A. & Thomas, J. M. (1996). *J. Phys. Chem.* **100**, 8977–8985.
- Bazin, D., Gucci, L. & Lynch, J. (2002). *Appl. Catal. A*, **226**, 87–113.
- Berry, F. J., Marco, J. F. & Steel, A. T. (1993). *J. Alloy. Comp.* **194**, 167–172.
- Broach, R. W., Bedard, R. L., Song, S. G., Pluth, J. J., Bram, A., Riekel, C. & Weber, H.-P. (1999). *Chem. Mater.* **11**, 2076–2080.
- Brunelli, M., Wright, J. P., Vaughan, G. B. M., Mora, A. J. & Fitch, A. N. (2003). *Angew. Chem. Int. Ed.* **42**, 2029–2032.
- Burla, M. C., Camalli, M., Cascarano, G., Giacovazzo, C., Polidori, G. R., Spagna, R. & Viterbo, D. (1989). *J. Appl. Cryst.* **22**, 389–393.
- Burton, A. & Elomari, S. (2004). *J. Chem. Soc. Chem. Commun.* pp. 2618–2619.
- Cassetta, A., Deacon, A. M., Ealick, S. E., Helliwell, J. R. & Thompson, A. W. (1999). *J. Synchrotron Rad.* **6**, 822–833.
- Cejka, J. (2002). *Catal. Rev.* **44**, 375–421.
- Cernik, R. J., Cheetham, A. K., Prout, C. K., Watkin, D. J., Wilkinson, A. P. & Willis, B. T. M. (1991). *J. Appl. Cryst.* **24**, 222–226.
- Cernik, R. J., Clegg, W., Catlow, C. R. A., Bushnell-Wye, G., Flaherty, J. V., Greaves, G. N., Burrows, I., Taylor, D. J., Teat, S. J. & Hamichi, M. (1997). *J. Synchrotron Rad.* **4**, 279–286.
- Cernik, R. J., Murray, P. K., Pattison, P. & Fitch, A. N. (1990). *J. Appl. Cryst.* **23**, 292–296.
- Cheetham, A. K., Ferey, G. & Loiseau, T. (1999). *Angew. Chem. Int. Ed.* **38**, 3268–3292.
- Cheetham, A. K. & Wilkinson, A. P. (1992). *Angew. Chem. Int. Ed. Engl.* **31**, 1557–1570.
- Christensen, A. N., Jensen, T. R., Norby, P. & Hanson, J. C. (1998). *Chem. Mater.* **10**, 1688–1693.
- Ciraola, M. F., Hanson, J. C., Norby, P. & Grey, C. P. (2001). *J. Phys. Chem. B*, **105**, 2604–2611.
- Clegg, W. (2000). *J. Chem. Soc. Dalton Trans.* pp. 3223–3232.
- Cowley, A. R., Jones, R. H., Teat, S. J. & Chippindale, A. M. (2002). *Micropor. Mesopor. Mater.* **51**, 51–64.
- Crick, F. H. C. & Magdoff, B. M. (1956). *Acta Cryst.* **9**, 901–908.
- Dalconi, M. C., Alberti, A. & Cruciani, G. (2003). *J. Phys. Chem. B*, **107**, 12973–12980.
- David, W. I. F., Shankland, K., McCusker, L. B. & Baerlocher, C. (2002). *Structure Determination from Powder Diffraction Data. IUCr Monographs on Crystallography 13*. Oxford University Press.
- David, W. I. F., Shankland, K. & Shankland, N. (1998). *Chem. Commun.* pp. 931–932.
- Davis, M. E. (2002). *Nature (London)*, **417**, 813–821.
- Dent, A. J., Greaves, G. N., Roberts, M. A., Sankar, G., Wright, P. A., Jones, R. H., Sheehy, M., Madill, D., Catlow, C. R. A., Thomas, J. M. & Rayment, T. (1995). *Nucl. Instrum. Methods Phys. Res. B*, **97**, 20–22.
- Dooryhee, E., Catlow, C. R. A., Couves, J. W., Maddox, P. J., Thomas, J. M., Greaves, G. N., Steel, A. T. & Townsend, R. P. (1991). *J. Phys. Chem.* **95**, 4514–4521.
- Einspahr, H. M., Suguna, K., Suddath, F. L., Ellis, G., Helliwell, J. R. & Papiz, M. Z. (1985). *Acta Cryst.* **B41**, 336–341.
- Evans, G. & Pettifer, R. F. (2001). *J. Appl. Cryst.* **34**, 82–86.
- Ferey, G. (2001). *Chem. Mater.* **13**, 3084–3098.

- Glaser, T., Hedman, B., Hodgson, K. O. & Solomon, E. I. (2000). *Acc. Chem. Res.* **33**, 859–868.
- Grosse-Kunstleve, R. W., McCusker, L. B. & Baerlocher, Ch. (1997). *J. Appl. Cryst.* **30**, 985–995.
- Harding, M. M. (1996). *J. Synchrotron Rad.* **3**, 250–259.
- Harris, K. D. M., Tremayne, M., Lightfoot, P. & Bruce, P. G. (1994). *J. Am. Chem. Soc.* **116**, 3543–3547.
- Hartman, M. (2000). *Angew. Chem. Int. Ed.* **39**, 888–890.
- Hartman, M. & Kevan, L. (1999). *Chem. Rev.* **99**, 635–663.
- Helliwell, J. R. (1992). *Macromolecular Crystallography with Synchrotron Radiation*. Cambridge University Press.
- Helliwell, M. (2000). *J. Synchrotron Rad.* **7**, 139–147.
- Helliwell, M., Helliwell, J. R., Cassetta, A., Hanson, J. C., Ericsson, T., Kvik, Å., Kaucic, V. & Frampton, C. (1996). *Acta Cryst.* **B52**, 479–486.
- Helliwell, M., Helliwell, J. R., Kaucic, V., Zabukovec Logar, N., Braba, L., Busetto, E. & Lausi, A. (1999). *Acta Cryst.* **B55**, 327–332.
- Henry, P. F., Weller, M. T. & Wilson, C. C. (2001). *J. Phys. Chem. B*, **105**, 7452–7458.
- Jones, R. H., Chen, J., Sankar, G. & Thomas, J. M. (1994). *Stud. Surf. Sci. Catal.* **84**, 2229–2236.
- Joubert, J.-M., Cerny, R., Latroche, M., Percheron-Guegan, A. & Yvon, K. (1998). *J. Appl. Cryst.* **31**, 327–332.
- Kariuki, B. M., Serrano-Gonzalez, H., Johnston, R. L. & Harris, K. D. M. (1997). *Chem. Phys. Lett.* **280**, 189–105.
- Kaucy, D., Vondrova, A., Dedecek, J. & Wichterlova, B. (2000). *J. Catal.* **194**, 318–329.
- Ko, Y., Kim, S. J., Kim, M. H., Park, J.-H., Parize, J. B. & Uh, Y. S. (1999). *Micropor. Mesopor. Mater.* **30**, 213–218.
- McCusker, L. B. (1991). *Acta Cryst.* **A47**, 297–313.
- Marcilly, C. (2001). *Stud. Surf. Sci. Catal.* **135**, 37–60.
- Marlow, F., Dong, W. T., Hoffmann, K. & Loerke, J. (2002). In *Handbook of Porous Solids*, Vol. 5, edited by F. Schuth, K. S. W. Sing and J. Weitkamp. Heidelberg: Wiley-VCH.
- Milanesio, M., Artioli, G., Gualtieri, A. F., Palin, L. & Lamberti, C. (2003). *J. Am. Chem. Soc.* **125**, 14549–14558.
- Muncaster, G., Sankar, G., Catlow, R. A., Thomas, J. M., Bell, R. G., Wright, P. A., Coles, S., Teat, S. J., Clegg, W. & Reeve, W. (1999). *Chem. Mater.* **11**, 158–163.
- Murray, A. D., Fitch, A. N. & Jouanneaux, A. (1990). *MPOFIL. A Program for Le Bail Decomposition of Powder Patterns*.
- Norby, P., Christensen, A. N. & Hanson, J. C. (1999). *Inorg. Chem.* **38**, 1216–1221.
- Norby, P. & Hanson, J. C. (1998). *Catal. Today*, **39**, 301–309.
- Novak Tusar, N., Mali, G., Arcon, I., Kaucic, V., Ghanbari-Shiankhali, A. & Dwyer, J. (2002). *Micropor. Mesopor. Mater.* **55**, 203–216.
- Novak Tusar, N., Zabukovec Logar, N., Arcon, I., Thibault-Starzyk, F. & Kaucic, V. (2001). *Croat. Chem. Acta*, **74**, 837–849.
- Novak Tusar, N., Zabukovec Logar, N., Arcon, I., Thibault-Starzyk, F., Ristic, A., Rajic, N. & Kaucic, V. (2003). *Chem. Mater.* **15**, 4745–4750.
- Ohsumi, K., Hagiya, K. & Ohmasa, M. (1991). *J. Appl. Cryst.* **24**, 340–348.
- Olczak, A., Cianci, M., Hao, Q., Rizkallah, P. J., Raftery, J. & Helliwell, J. R. (2003). *Acta Cryst.* **A59**, 327–334.
- Peter, S., Cockcroft, J. K., Roisnel, T. & Lutz, H. D. (1996). *Acta Cryst.* **B52**, 423–427.
- Rajic, N., Zabukovec Logar, N., Mali, G. & Kaucic, V. (2003). *Chem. Mater.* **15**, 1734–1738.
- Ressler, T., Brock, S. L., Wong, J. & Suib, S. L. (1999). *J. Synchrotron Rad.* **6**, 728–730.
- Ristic, A., Novak Tusar, N., Arcon, I., Zabukovec Logar, N., Thibault-Starzyk, F., Czyzniewska, J. & Kaucic, V. (2003). *Chem. Mater.* **15**, 3643–3649.
- Roberts, M. A., Sankar, G., Thomas, J. M., Jones, R. H., Du, H., Chen, J., Pang, W. & Xu, R. (1996). *Nature (London)*, **381**, 401–404.
- Round, C. I., Williams, C. D. & Duke, C. V. A. (1997). *Chem. Commun.* pp. 1849–1850.
- Sankar, G., Rey, F., Thomas, J. M., Greaves, G. N., Corma, A., Dobson, B. R. & Dent, A. J. (1994). *Chem. Commun.* pp. 2279–2280.
- Sankar, G., Thomas, J. M., Rey, F. & Greaves, G. N. (1995). *Chem. Commun.* pp. 2549–2550.
- Schmidt, S., Poulsen, H. F. & Vaughan, G. B. M. (2003). *J. Appl. Cryst.* **36**, 326–332.
- Shankland, K., David, W. I. F. & Csoka, T. (1997). *Z. Kristallogr.* **212**, 550–552.
- Shankland, K., David, W. I. F. & Sivia, D. S. (1997). *J. Mater. Chem.* **7**, 569–572.
- Sheldrick, G. M. (1985). In *Crystallographic Computing*, Vol. 3, edited by G. M. Sheldrick, C. Kruger and R. Goddard. Oxford University Press.
- Szostak, R. (1998). *Synthesis of Molecular Sieve Phosphates, Molecular Sieves Science and Technology*, Vol. 1, *Synthesis*, edited by H. G. Karge and J. Weitkamp, pp. 157–185. Berlin/Heidelberg: Springer-Verlag.
- Thomas, J. M. & Sankar, G. (2001). *J. Synchrotron Rad.* **8**, 55–60.
- Tremayne, M., Kariuki, B. M. & Harris, K. D. M. (1997). *Angew. Chem. Int. Ed.* **36**, 770–772.
- Tuel, A., Arcon, I., Novak Tusar, N. & Kaucic, V. (1996). *Micropor. Mater.* **7**, 271–284.
- Visser, J. W. J. (1969). *Appl. Cryst.* **2**, 89.
- Walton, R. I., Norquist, A., Smith, R. I. & O'Hare, D. (2002). *Faraday Discuss.* **122**, 331–341.
- Walton, R. I. & O'Hare, D. (2000). *Chem. Commun.* pp. 2283–2291.
- Wilson, S. T., Lok, B. M., Messina, C. A., Cannan, T. R. & Flanigen, E. M. (1982). *J. Am. Chem. Soc.* **104**, 1146–1147.